

Magnetic interactions in transition-metal doped ZnO: An ab-initio study

Priya Gopal and Nicola A. Spaldin
Materials Department
University of California, Santa Barbara,
California 93106-5050, USA

(Dated: February 6, 2008)

We calculate the nature of magnetic interactions in transition-metal doped ZnO using the local spin density approximation and LSDA+ U method of density functional theory. We investigate the following four cases: (i) single transition metal ion types (Cr, Mn, Fe, Co, Ni and Cu) substituted at Zn sites, (ii) substitutional magnetic transition metal ions combined with additional Cu and Li dopants, (iii) substitutional magnetic transition metal ions combined with oxygen vacancies and (iv) pairs of magnetic ion types (Co and Fe, Co and Mn, etc.). Extensive convergence tests indicate that the calculated magnetic ground state is unusually sensitive to the k-point mesh and energy cut-off, the details of the geometry optimizations and the choice of the exchange-correlation functional. We find that ferromagnetic coupling is sometimes favorable for single type substitutional transition metal ions within the local spin density approximation. However, the nature of magnetic interactions changes when correlations on the transition-metal ion are treated within the more realistic LSDA + U method, often disfavoring the ferromagnetic state. The magnetic configuration is sensitive to the detailed arrangement of the ions and the amount of lattice relaxation, except in the case of oxygen vacancies when an antiferromagnetic state is always favored.

PACS numbers:
Keywords:

I. INTRODUCTION

Dilute magnetic semiconductors (DMSs), obtained by partial replacement of the cations in conventional semiconductors by magnetic transition-metal ions, are of current interest as potential semiconductor-compatible magnetic components for spintronic applications¹. Early studies of DMSs focussed on II-VI semiconductor hosts such as CdSe and ZnTe²; since many transition metals adopt divalent ionic states, they therefore substitute readily for divalent cations such as Zn²⁺ or Cd²⁺. However, most II-VI DMSs are antiferromagnetic or have very low ferromagnetic Curie temperatures³, rendering them unattractive for applications. More recently, robust ferromagnetism was observed in DMSs based on III-V semiconductors such as Mn-doped GaAs, in which Curie temperatures of ~ 150 K have been achieved⁴. Here, the ferromagnetic coupling between the localized Mn magnetic moments is believed to be mediated by itinerant carriers (holes) which are introduced when divalent Mn ions replace trivalent galliums^{5,6} (so-called *carrier-mediated ferromagnetism*). Calculations for other materials, based on such a carrier-mediated mechanism with a high concentration (~ 5 %) of holes, predicted above-room-temperature ferromagnetism for Mn-doped ZnO and GaN⁵.

In addition to the technological appeal of room-temperature ferromagnetism in ZnO-based DMSs, ZnO offers other desirable features as a semiconductor host. It has a direct wide band gap of 3.3 eV⁷, and therefore finds widespread use in the optoelectronics industry^{8,9,10}. Its strong piezoelectricity¹¹ is exploited in a variety of transducer applications¹² and have possible application

in polarization field effect transistors¹³. And long spin coherence times, with potential spintronic applications, have recently been reported at room temperature in n-type ZnO¹⁴. Thus, if it could be achieved, ferromagnetic ZnO would be a highly multifunctional material with co-existing (and possibly coupled) magnetic, piezoelectric, optical and semiconducting properties.

The predictions of high-temperature ferromagnetism⁵ spawned a large number of experimental^{15,16,17,18,19,20,21,22,23,24,25} and computational^{26,27,28,29,30,31,32} studies of transition-metal (TM)-doped ZnO. The reported experimental values of Curie temperature and magnetization show a large distribution, suggesting that the system is sensitive to preparation methods, measurement techniques, substrate choice, etc. For example, in the case of Mn-doped ZnO, while some experiments report above room temperature ferromagnetism^{20,33}, others report a low ferromagnetic ordering temperature^{19,34,35} or a spin-glass or paramagnetic behavior^{18,22,36}. Likewise, in Co-doped ZnO, there are reports of giant magnetic moments ($\sim 6.1 \mu_B/\text{Co}$)²¹, high ferromagnetic ordering temperatures with moments of $\sim 1-3 \mu_B$ ^{16,37,38,39} and in some cases no ferromagnetic behavior at all^{22,25,36,40}. Interestingly, the reported computational results show a similar spread of values; this arises in part from different physical approximations (choice of exchange-correlation functional, inclusion or omission of structural relaxations), but also from the unusual sensitivity of the magnetic interactions to the convergence quality of the computations. (For a detailed review see Ref. 24). As a result, in spite of the flurry of experimental and theoretical work, no definite conclusions have been

reached regarding the nature and origin of the magnetic interactions in this system.

In this work, we report our results of a systematic computational study of transition-metal-doped ZnO, with the goal of understanding the nature and origin of the magnetic interactions. Our emphasis is on extracting trends along the $3d$ transition metal series, and so we first explore the effects of substitutional doping with a range of transition metals (Cr, Mn, Fe, Co, Ni and Cu). Next, we calculate the effects of additional dopant or vacancy impurities, and finally we calculate the preferred magnetic configurations of *pairs* of different magnetic ion types. Our main finding is that the ferromagnetic state is generally disfavored in the most realistic calculations, and it is not strongly stabilized by common defects likely to be found in as-grown ZnO, or easily incorporated as dopants.

The remainder of this paper is organized as follows. In the next section, we describe our computational and system details and outline the unusually demanding convergence behavior that we find for TM-doped ZnO. In Sec. III, we present our calculated trends across the $3d$ series for single-type transition metal doping within the local spin density approximation (LSDA) and the LSDA+ U method. In Sec. IV we investigate the influence of defects across the $3d$ series by (i) co-doping with Cu or Li and (ii) incorporation of oxygen additional oxygen vacancies. In Sec. V, we present our results for double doping (simultaneous doping of two different TM ions) in (Zn,(Co,Fe))O and (Zn,(Mn,Co))O. Finally, we summarize our results in Sec. VI

II. TECHNICALITIES

A. System details

In order to achieve realistic experimental dopant concentrations ($\sim 10 - 30\%$), we used a periodic $2 \times 2 \times 2$ wurtzite supercell of ZnO which consists of 32 atoms in a unit cell. Substitution of two Zn atoms by transition metal ions then gives a dopant concentration of 12.5% and allows for calculation of the relative energies of ferromagnetic (FM) and antiferromagnetic (AFM) orderings. We explored two spatial arrangements, *near* (transition metal atoms separated by one oxygen atom) and *far* (TM atoms separated by -O-Zn-O-), as shown Figure 2. In each case, we used the energy difference between FM and AFM ordering, $\Delta E = E_{AFM} - E_{FM}$, as an indicator of the magnetic stability (a positive ΔE implies that FM is favorable). Equating ΔE with the thermal energy $k_B T$ suggests room temperature ferromagnetism should be achieved for ΔE values larger than ~ 30 meV.

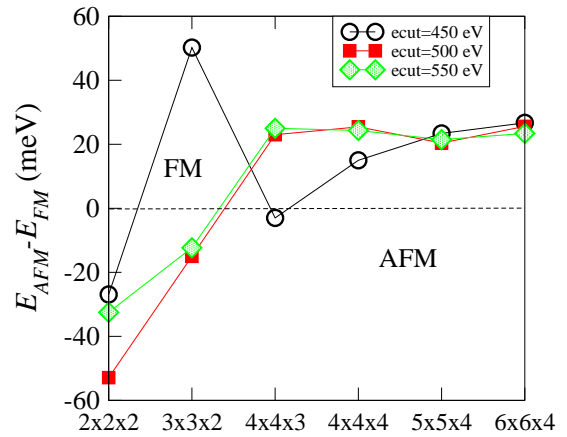


FIG. 1: Plot of $E_{AFM} - E_{FM}$ for $Zn_{0.875}Co_{0.125}O$ as a function of k-point grid, and for three different plane-wave energy cut-offs (ecut).

B. Method details

Our total energy and electronic structure calculations were performed using the projector augmented wave (PAW)⁴¹ formalism of density functional theory as implemented in the VASP package^{42,43,44}. We used the default VASP PAW potentials with 12 valence electrons for Zn ($3d^{10}4s^2$), 6 for O ($2p^42s^2$) and $2+n$ ($3d^n4s^2$; $n = 3$ to 9) for the transition metals. We used a well converged energy cut-off of 550 eV for plane-wave expansion of the PAW's, a $4 \times 4 \times 3$ Gamma centered k-point grid, and the tetrahedron method with Blöchl⁴¹ corrections for the Brillouin Zone integrations. Note that this energy cut-off and k-point sampling are unusually high; our convergence tests (Figure 1 indicate that qualitatively incorrect magnetic behavior often occurs for lower values. Similarly rigorous convergence parameters have been shown to be required for accurate calculations for Co-doped TiO_2 ⁴⁵. For all geometry optimizations, we kept the volume of the supercell fixed to the experimental volume ($a=6.50\text{\AA}$ and $c=10.41\text{\AA}$) and relaxed all the internal coordinates until the Hellman-Feynman forces were less than 10^{-3} eV/Å.

We approximated the exchange-correlation functional with both the local spin density approximation (LSDA) and the fully localized limit of the LSDA+ U method⁴⁶. Although widely used and well established for many properties, the LSDA is well-known to yield incorrect behavior for strongly correlated magnetic systems, often predicting half-metallic, low spin states for systems which are actually insulating and high spin. For example, most TM monoxides are wide band gap antiferromagnetic insulators^{47,48,49,50,51}, however the LSDA finds them to be either FM metals (FeO and CoO) or small-gap semiconductors (MnO and NiO)⁵². The LSDA+ U method extends the LSDA by explicitly adding the on-site $d-d$ Coulomb interaction, U , and the on-site exchange inter-

action, J , to the LSDA Hamiltonian, and usually gives improved results for magnetic insulators. Here we use typical values of $U = 4.5$ eV and $J = 0.5$ eV on all transition metals^{53,54,55}; although a small variation in U and J across the series is expected, our choice of constant values permits a more straightforward comparison. We do not modify the LSDA ZnO electronic structure, which therefore shows the usual LSDA underestimation of the band gap, and underestimation of the Zn d state energies.

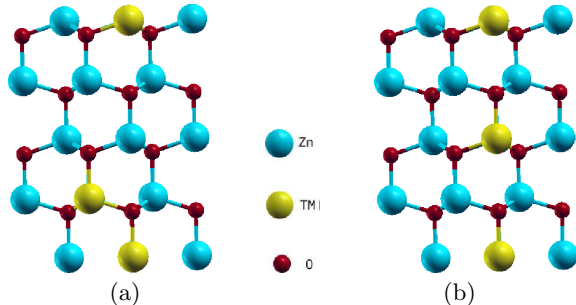


FIG. 2: (Color online) Wurtzite supercell of ZnO with two TM ions in the (a) near and (b) far configuration. The (yellow) light-shaded spheres are the TM ions, the large (cyan) dark-shaded spheres the Zn ions, and the small (red) black spheres the O ions.

III. MAGNETIC INTERACTIONS IN DOPED ZNO

A. LSDA results

We begin by calculating the total energies of 12.5% TM-substituted ZnO within the local spin density approximation (LSDA). We reiterate that we do not expect the LSDA to give accurate magnetic behavior for this system, but present the results as a baseline for comparison with our LSDA+ U results in the next section. Keeping the volume fixed at the ZnO experimental volume, we first relax all internal coordinates for *near* and *far* arrangements of the TM ions, and for both AFM and FM orderings. In figure 3 we show our calculated energy differences between the near and far configurations; it is clear that in all cases (except Mn, for which the energy difference is negligible) it is favorable for the TM ions to cluster together.

Figures 4(a) and (b) show our calculated magnetic energy differences ($E_{AFM} - E_{FM}$) for our range of TM dopants in the *near* and *far* spatial arrangements. First we note that our calculated magnetic orderings without ionic relaxations, which vary considerably both with the TM type and with the spatial arrangement, are consistent with earlier calculations in the literature^{17,27,56}. We see, however, that the strength and sign of the magnetic interaction is highly sensitive to the ionic relaxation, which changes both the distance between the TM

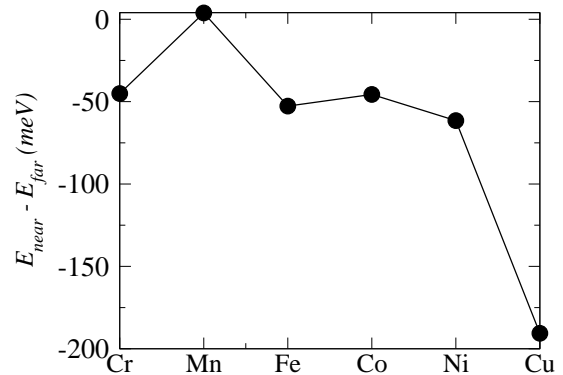


FIG. 3: LSDA energy differences ($\Delta E = E_{near} - E_{far}$) for substitutional TM ions. The negative energy difference indicates that the TM ions prefer to be in a *near* spatial configuration.

ions (by up to ~ 0.25 Å) and the TM-O-TM angle (by up to $\pm 5\%$). We find no clear trends in the magnitude of relaxation, nor any direct correlation between the relaxation and the change in the magnetic interactions, across the TM series. We attribute the sensitivity in magnetic ordering to a subtle competition between antiferromagnetic superexchange (favored by 180° bond angles), ferromagnetic superexchange (favored by 90° TM-O-TM bond angles) and AFM direct exchange (favored by short TM-TM distances)^{57,58,59}. Our results indicate that ionic relaxations must always be included in calculations to obtain meaningful results, and that even the generalization of relaxed positions from one TM ion to another should be applied with caution^{17,56}. For the most realistic configurations (*near*, with relaxations), the LSDA suggests that doping with Cr, Fe, Co, Ni and Cu should lead to a ferromagnetic ground state.

Next (Figure 5) we compare our calculated total densities of states (DOS) and TM $3d$ projected local densities of states (PDOS) for our range of TM ions in ZnO. In all cases the DOS for the FM arrangement is shown. The total DOS is represented by the gray shaded region while the black shaded regions represent the $3d$ states of the TM impurities. The majority (\uparrow) spin states are plotted along the negative x direction, and the minority (\downarrow) states are plotted along the positive x direction. The energies are reported relative to the Fermi energy ($E_f=0$). For comparison, the DOS of undoped ZnO is also shown, with the Fermi energy set to the top of the valence band.

Comparison with the ZnO DOS identifies the broad (~ 4 -5 eV) band just below the Fermi energy as derived largely from the O $2p$ states, with the narrow Zn $3d$ band just below and slightly overlapping with the O bands. The bottom of the conduction band is composed largely of Zn $4s$ states, and the band gap (~ 0.78 eV) shows the usual LSDA underestimation.

In all cases, the exchange-split TM $3d$ states form fairly narrow bands in the region of the gap. The exchange

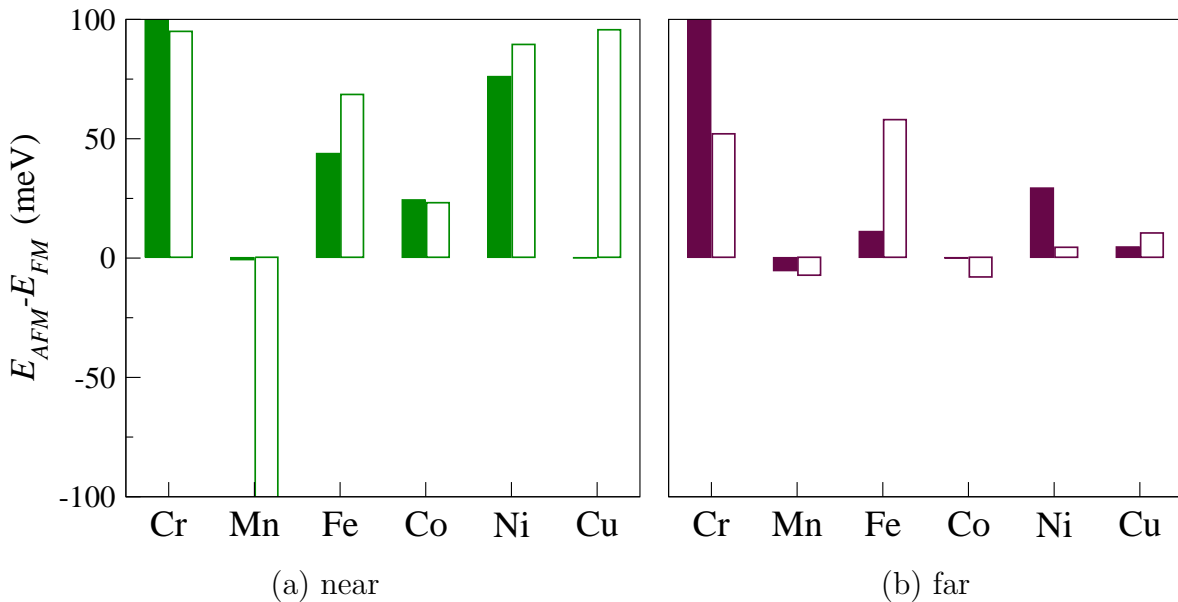


FIG. 4: LSDA energy differences ($\Delta E = E_{AFM} - E_{FM}$) for substitutional TM ions in ZnO for (a) *near* and (b) *far* spatial configurations. In both (a) and (b), the filled bars represent the case when the ionic coordinates are not relaxed and the unfilled bars represent the case when the ionic coordinates are relaxed. Lines at $\Delta E = 0$ indicate that FM and AFM orderings are equivalent in energy.

splitting (~ 2 eV) is consistently larger than the crystal field splitting (~ 0.5 eV) which splits each spin manifold into lower energy doubly degenerate e and higher energy triply degenerate t states. We observe the following trends, which are consistent with the crystal chemistry of 3d transition metal oxides:

- The energy of the TM 3d states relative to the top of the valence band shifts down in energy on moving right across the 3d series (from Cr to Cu). As a consequence, the Cr states are somewhat hybridized with the bottom of the conduction band (this is likely a result of the LSDA underestimation of the ZnO band gap), the Fe and Co states are largely mid-gap, and the Cu states are hybridized with the top of the valence band.
- The calculated DOSs (Figure 5) are consistent with the Hund's rule predictions for isolated TM ions, with only majority-spin (\uparrow) states occupied for Cr and Mn, and occupation of the minority-spin (\downarrow) states increasing Fe to Co to Ni to Cu. Also the exchange splitting decreases on moving to the right across the 3d series.
- The $(d^5)^\uparrow$ Mn²⁺ ion, and $(d^5)^\uparrow (d^2)^\downarrow$ Co²⁺ ions lead to insulating behavior; the other ions have partially filled d manifolds and a finite density of states at the Fermi level.
- The variation in magnetic moments across the 3d series reflects the decrease in exchange splitting,

and the increase in number of electrons, with the local magnetic moments (obtained by integrating up to a Wigner-Swartz radius of 1.4 \AA)⁶⁰ on the TM ion as follows (in units of μ_B): 3.04 (Cr), 4.31 (Mn), 3.51 (Fe), 2.44 (Co), 1.49 (Ni) and 0.55 (Cu).

These LSDA results are consistent with earlier LSDA calculations^{17,27,29}, and also with some experimental reports²⁰. Since the LSDA is known to underestimate the band gaps and exchange splittings in magnetic systems, we withhold a detailed analysis of the band structures until the next section, where we repeat our calculations with the inclusion of correlations at the level of the LSDA + U method.

B. LSDA + U

Next we repeat the suite of calculations described above, with the correlation on the 3d TM ions treated within the LSDA + U scheme⁴⁶. Here we present results obtained using typical values of $U = 4.5$ eV and $J = 0.5$ eV; in the appendix we discuss the U -dependence of our calculated properties.

First, in Figure 6 we present our calculated LSDA+ U DOSs of TM-doped ZnO. Although all the trends across

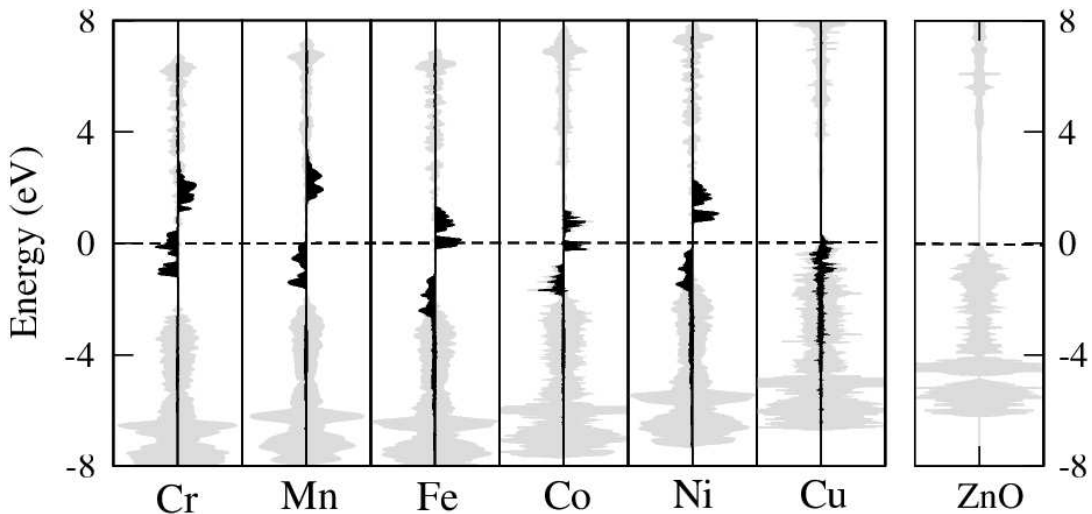


FIG. 5: DOS and PDOS of TM-doped ZnO with the TM atoms in the *near* spatial configuration calculated within the LSDA. The black shaded regions show the TM *d* states, and the gray shaded regions show the total DOS. For clarity, the TM *d* states are scaled by a factor of two. Also shown (right panel) is the DOS for undoped ZnO.

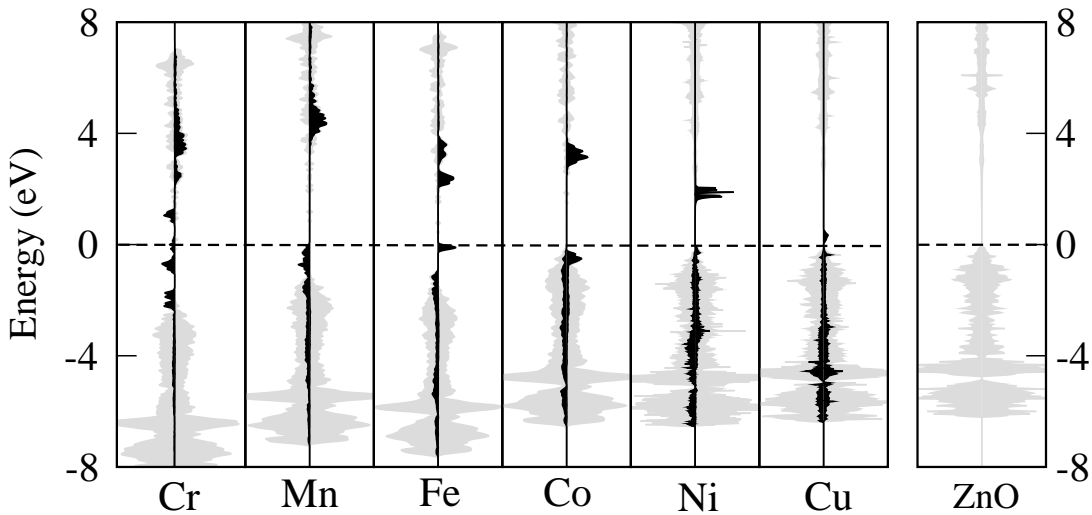


FIG. 6: DOS and PDOS of TM-doped ZnO with TM atoms in the *near* spatial configuration calculated within the LSDA + U method. The black shaded regions show the TM *d* states, and the gray shaded regions show the total DOS. For clarity, the TM *d* states are scaled by a factor of two. Also shown (right panel) is the DOS for undoped ZnO.

the series remain the same as in the LSDA, the addition of the Hubbard U term, as expected, causes an increased splitting between the filled and empty orbitals in the TM *d* manifold. The exchange splitting is now increased to ~ 4 eV, and the crystal-field splitting increases to ~ 1 eV. The TM *d* states, which were localized in the gap in the LSDA, now shift down in energy and hybridize strongly with the O $2p$ states. Comparing the DOS of Fe and Ni, we observe a transition from half-metallic to insulating when going from the LSDA to LSDA + U . This is directly reflected in the magnetic interaction strength. For e.g., in Fe and Ni, the long-range interaction vanishes and the interaction strength decreases. We also calculated the magnetic moments on the TM ion as follows (in units

of μ_B): 3.40 (Cr), 4.41 (Mn), 3.54 (Fe), 2.56 (Co), 1.63 (Ni) and 0.65 (Cu). The magnetic moments are slightly larger compared to the LSDA values. Next we compare the total energies of the FM and AFM magnetic orderings in the *near* and *far* spatial configurations. In all cases, all the ionic coordinates are relaxed within the LSDA + U scheme. Figures 7(a) and (b) show the energy difference between the FM and AFM states, $(E_{AFM} - E_{FM})$, for *near* and *far* arrangements for the various TM ions. As in the LSDA case, ΔE shows a strong dependence on the spatial arrangement of the dopant ions, as well as on the extent of ionic relaxations included in the calculation. In all cases, the sign and magnitude of the interactions are strikingly different from those obtained within the

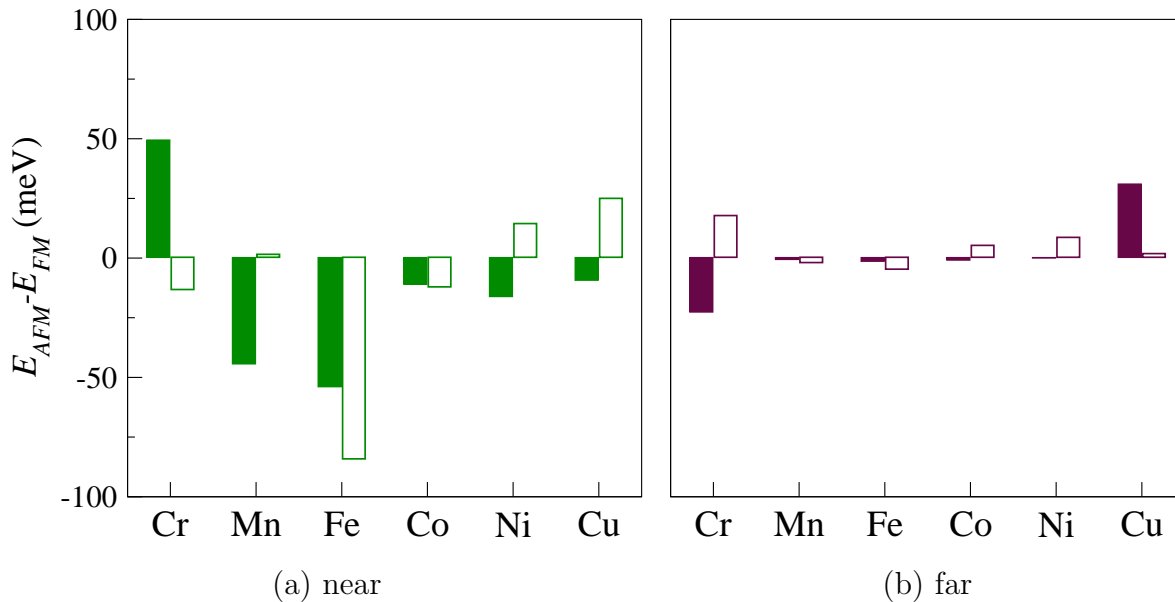


FIG. 7: LSDA $+U$ energy difference, $\Delta E = E_{AFM} - E_{FM}$, for substitutional TM ions in ZnO represented for (a) *near* and (b) *far* spatial configurations. The filled bars show the energies when the ions are not relaxed and the shaded bars give the values for when relaxations are included. Lines at $\Delta E = 0$ indicate that FM and AFM orderings are equivalent in energy.

LSDA, with a general trend to reduced ferromagnetism. For the energetically favorable *near* case, only Ni and Cu dopants show a tendency to ferromagnetic ordering when ionic relaxations are included in the calculation.

IV. INFLUENCE OF DEFECTS

A. Possible *p*-type dopants; Cu and Li with TM in ZnO

Given that our calculations containing single types of substitutional dopants are unable to reproduce the experimentally reported ferromagnetism, we next search for other impurities that could mediate the ferromagnetic ordering. Since the original predictions of high Curie temperature in Mn-doped ZnO⁵ assumed high hole concentrations, we first include additional dopants which are likely to introduce *p*-type carriers. Some experimental⁶¹ and theoretical studies⁵⁶ have suggested that Cu could provide holes when doped into ZnO. Cu has an electronic configuration of $3d^9 4s^2$, and has a tendency to form Cu^{1+} ions with a $3d^{10} 4s^0$ electron configuration, and an ionic radius (0.60 Å) close to that of Zn^{2+} . Thus it is reasonable to assume that substitution of Zn with Cu could yield a Cu^{1+} configuration with an associated hole. Indeed, earlier LSDA calculations on Cu-doped ZnO found a band structure consistent with this model, and an enhanced tendency to ferromagnetism²⁹. Lithium has also been suggested as a possible *p*-type dopant in ZnO⁶². Li has an electronic configuration of $1s^2, 2s^1$, and, like Cu,

tends to form a singly charged cation ($1s^2 2s^0$) with an ionic radius (0.59 Å) close to that of Zn^{2+} . In this section, we calculate the effects of co-doping TM-doped ZnO with Cu or Li, again within the LSDA+U method, using the same convergence and U and J parameters as described above. Our calculated ΔE values are shown in figure 8. In all cases the concentration of the Cu or Li was 6.25% (one additional dopant in 16 cations), and the additional dopant was placed far away from the TM ion in ZnO. It is clear that, in contrast with earlier LSDA calculations, co-doping with Cu within the LSDA+U method does not strongly enhance the tendency towards ferromagnetism, yielding an antiferromagnetic ground state in most cases, and a weakly ferromagnetic state for Cr and Ni. Co-doping with Li, however, is more favorable, and in some cases should lead to above-room-temperature ferromagnetism. This is particularly intriguing in light of recent reports of ferroelectricity in Li-doped ZnO^{63,64}, suggesting the possibility of engineering a multiferroic material with simultaneous ferromagnetism and ferroelectricity. However, none of our calculated Li-doped materials is insulating, a requirement for ferroelectricity.

B. O vacancies: Zn(TM, V_o)O

Next, we combine substitutional TM ions with oxygen vacancies, which are believed to be the most common native defects in ZnO^{62,65,66}. There is some ex-

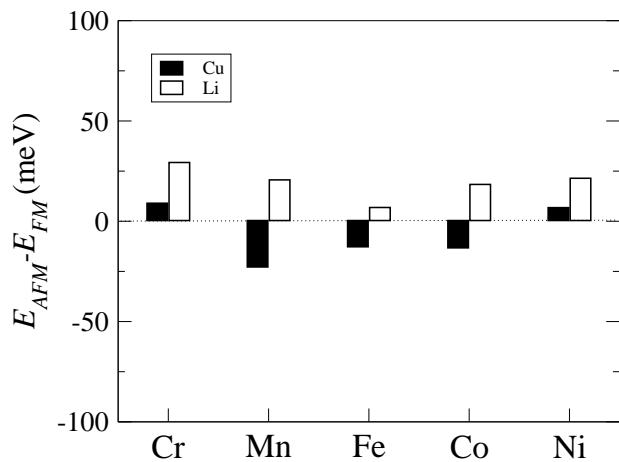


FIG. 8: $E_{AFM} - E_{FM}$ for TM-doped ZnO with 6.25% Cu/Li.

perimental evidence associating the presence of oxygen vacancies with the existence of ferromagnetism in TM-doped ZnO. For example, Venkatesan¹⁶ *et al.* reported a correlation between the magnitude of Co magnetic moments and the oxygen partial pressure during annealing, with higher oxygen partial pressure reducing the amount of magnetization. In addition, Kittilsved *et al.*²³ report the observation of room-temperature ferromagnetism in Co-doped ZnO nanocrystals with oxygen-containing surfaces, and propose that oxygen vacancies mediate the magnetic interactions. A couple of experiments also observe a change in the magnetization in samples annealed in reduced atmospheric pressures and they attribute it to oxygen vacancies⁶⁷. As a result of this reported correspondence between the presence of oxygen vacancies and the existence of ferromagnetism, a model has been proposed in which ferromagnetism is mediated by carriers in a spin-split impurity band derived from extended donor orbitals^{16,37}. The validity of the model rests on the formation of an oxygen-vacancy-derived donor impurity band close to the ZnO conduction band edge, which hybridizes with the spin-polarized TM $3d$ band. If the Fermi energy lies within this hybrid oxygen vacancy/TM $3d$ spin-polarized band, a carrier-mediated ferromagnetism should be favorable. Here we calculate the relative energies of the oxygen impurity levels and the transition metal $3d$ states across the TM series, in order to investigate the applicability of this model. Indeed, by simple charge neutrality arguments, removal of a neutral oxygen atom should leave two unbonded electrons associated with the vacancy, provided that the Zn remains in a Zn^{2+} state. We note, however, that recent first-principles calculations⁶⁸ found oxygen vacancies to be deep donors in ZnO, and therefore unavailable for carrier mediation.

We introduce a single O vacancy as far as possible from the TM ions which are again in both the *near* and *far* configurations. The energy difference ($E_{AFM} - E_{FM}$) is plotted in Figure 9. We see that the AFM state is stable in all cases, consistent with previous computations for

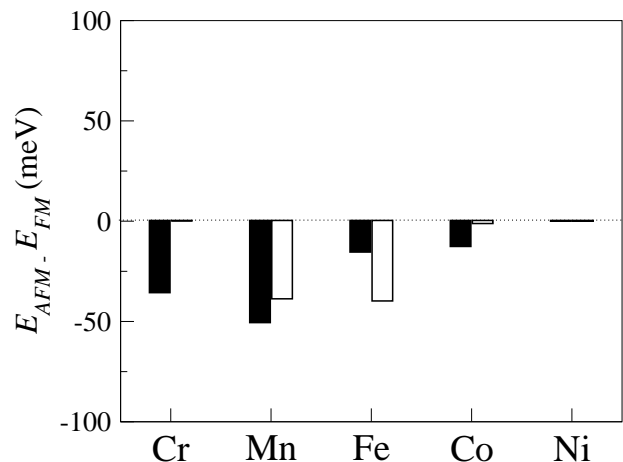


FIG. 9: $E_{AFM} - E_{FM}$ for the range of TM ions in the presence of an oxygen vacancy. The shaded and unshaded bars represent the cases when the TM ions are *near* and *far* from each other respectively. In both cases the oxygen vacancy is placed as far as possible from the TM ions.

Co-doped ZnO with a neutral oxygen vacancy^{17,29,30}.

In Figure 10 we show our calculated DOSs for the entire series. Note that the defect concentration used in our calculations is higher than likely attainable experimentally ($\sim 1-2\%$), but that the relative band alignments will be largely unchanged by the increased concentration. We see a shift of the Fermi energies relative to those in the absence of oxygen vacancies, but no other striking changes in band structure. In particular, it is clear that the Fermi level does not lie in a hybridized TM $3d$ -O $2p$ impurity band for any case. Therefore our band structures are not consistent with those required to mediate ferromagnetism within the model proposed above; they are however consistent with our calculated AFM ground states.

The calculated magnetic moments (in units of μ_B) for each TM ion in the presence of the oxygen vacancy are 3.54 (Cr), 4.36 (Mn), 3.66 (Fe), 2.64 (Co) and 1.68 (Ni), largely unchanged from the LSDA+U values without the oxygen vacancy. This indicates that the two electrons from the oxygen vacancy are localised and do not influence the occupancy of the TM d states. Finally, we point out that we have considered only neutral oxygen vacancies here. A recent first principles study suggests that positively charged oxygen vacancies might be more successful for mediating ferromagnetism in Co-doped ZnO³⁰.

C. Other defects

Next, we study the effect of a range of experimentally plausible defects – Zn vacancies (V_{Zn}), octahedral Zn interstitials (Zn_i), TM interstitials (Co_i) and Li interstitials (Li_i) – on the magnetic interactions. Rather than

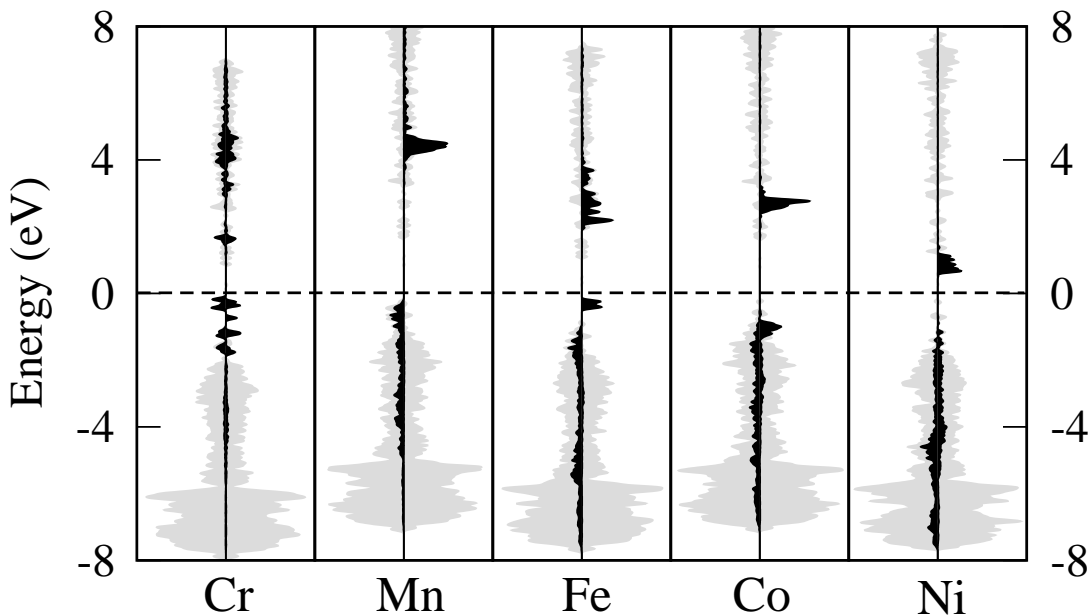


FIG. 10: DOS and PDOS for TM-doped ZnO (*near* spatial arrangement and FM state) in the presence of oxygen vacancies.

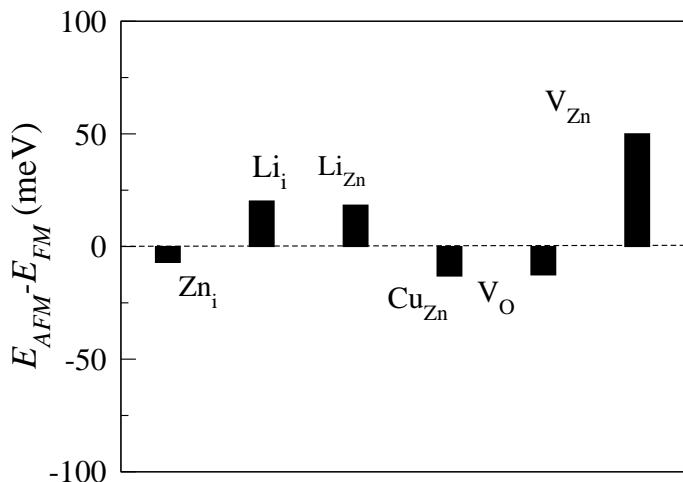


FIG. 11: $E_{AFM} - E_{FM}$ for ZnO doped with Co and a range of other defects.

scanning the entire range of transition metal dopants, we use Co-doped ZnO as our test system, since it is the most widely studied both experimentally^{15,16,24,69,70} and theoretically^{17,29,30,56,71}. Figure 11 shows our calculated $\Delta E = E_{AFM} - E_{FM}$ for the *near* spatial arrangement, with the vacancies placed as far as possible from the Co ions. Our previously reported values for substitutional Li (Li_{Zn}) and oxygen vacancies (V_O) are also shown for completeness.

Perhaps the most important result is that, as in the case of substitutional Li reported above, interstitial Li also sta-

bilizes the ferromagnetic state. This is significant since Li impurities are likely to be incorporated both in substitutional and interstitial sites during growth, and avoiding competing antiferromagnetic interactions is desirable. We also see that Zn vacancies are favorable for ferromagnetism, consistent with previous reports in the literature^{17,29,30}. The other defects studied do not stabilize the ferromagnetic state.

V. SIMULTANEOUS DOPING OF CO WITH OTHER TM IONS

Finally, we calculate the properties of ZnO doped with both Co and an additional TM ion (Mn or Fe). There has been some experimental work on such co-doped ZnO-based DMSs. Cho⁷⁰ *et al.* reported room-temperature magnetism with a saturation magnetization of 5.4 emu/g (corresponding to $\sim 1\mu_B$ for CoFe pair) for $Zn_{1-x}(Fe_{0.5},Co_{0.5})_xO$ ($x=0.15$) films fabricated by reactive magnetron co-sputtering. Han⁶¹ *et al.* also reported room temperature magnetism for $Zn_{1-x}(Fe_{1-y},Cu_y)_xO$ bulk samples with $T_C \sim 550K$. On the theory side, Park and Min²⁶ calculated the electronic structures and magnetic properties of (Fe,Co) and (Fe,Cu) doped ZnO at 12.5% doping. They reported a tendency to form FM Fe-O-Cu clusters, and argued that ferromagnetism should arise from double exchange, whereas the absence of clustering found for (Fe,Co)-doped ZnO would require a different mechanism for ferromagnetism.

Here we explore the possibility of ferrimagnetic (FiM) ordering, in which the magnetic moments of one TM ion type are antiparallel to those of the other TM ion type, but a net magnetization arises from incomplete

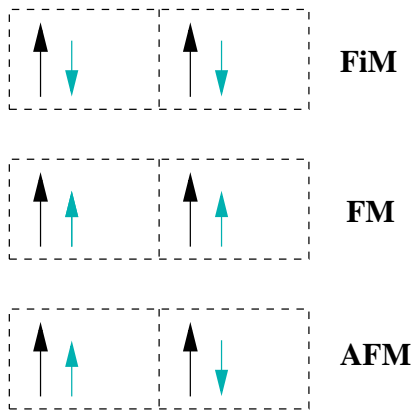


FIG. 12: (Color online) A schematic of the different magnetic orderings investigated in this work. The black arrows represent the magnetic moments of the Co ions while the blue (gray) arrow represent the magnetic moment of the other TM ion (Mn or Fe).

cancellation of the magnetic moments. For each system ($\text{Zn}(\text{Co,Fe})\text{O}$, $\text{Zn}(\text{Co,Mn})\text{O}$) we calculate the total energies of the FM, AFM and FiM magnetic orderings as shown in Figure 12 with TM ions of different type in the *near* arrangement. We use a $4 \times 4 \times 2$ wurtzite supercell with 64 atoms (double the size of the previous studies), which allows the permutations shown in Figure 12 at a TM ion concentration of 12.5%. Within this constrained spatial arrangement, we find that in both systems the FiM ordering is the most stable arrangement by 200 meV for $(\text{Zn},(\text{Co,Fe}))\text{O}$, and by 57 meV for $(\text{Zn},(\text{Co,Mn}))\text{O}$; the corresponding magnetic moments per supercell are $1.11 \mu_B$ for $(\text{Zn},(\text{Co,Fe}))\text{O}$ and $1.98 \mu_B$ for $(\text{Zn},(\text{Co,Mn}))\text{O}$ which agrees well with the experimentally reported values⁷⁰. While ferrimagnetism overcomes the problem of cancellation of magnetic moments by superexchange-driven antiparallel alignment, it of course requires that ions of different types cluster together while those of the same type remain distant; this might be difficult to achieve experimentally.

For completeness, we show the DOSs of FiM $\text{Zn}_{0.875}(\text{Co}_{0.5}\text{M}_{0.5})_{0.125}\text{O}$ ($M = \text{Mn}, \text{Fe}$) in Figure 13. The $(\text{Zn},(\text{Mn,Co}))$ DOS is almost an exact superposition of the separate $(\text{Zn},\text{Mn})\text{O}$ and $(\text{Zn},\text{Co})\text{O}$ DOSs. Interestingly, in the $(\text{Zn},(\text{Fe,Co}))\text{O}$ system, we get a metallic state because of the narrow band spin polarized impurity band at the Fermi level unlike either $(\text{Zn},\text{Fe})\text{O}$ or $(\text{Zn},\text{Co})\text{O}$. The Coey model described in the previous section could be appropriate in this picture where the donor impurity band of one the transition metal atom (in this case Fe) lies close to the conduction band edge and overlaps with the Fermi level. Thus we have a stable ferrimagnetic state.

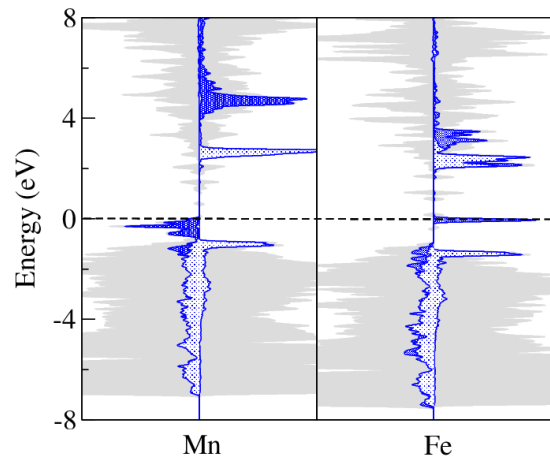


FIG. 13: DOSs and PDOSs of $3d$ states for ferrimagnetic $\text{Zn}_{0.875}(\text{Co}_{0.5}\text{Mn}_{0.5})_{0.125}\text{O}$ and $\text{Zn}_{0.875}(\text{Co}_{0.5}\text{Fe}_{0.5})_{0.125}\text{O}$. The blue shaded region represents the d states of the Co ions while the red shaded region represents the d states of the TM ions.

VI. SUMMARY

In summary, we have performed a systematic study of the magnetic behavior of TM-doped ZnO for a range of TM ions and defects. Our main result is the absence, in general, of a tendency for pairs of TM ions substituted for Zn to order ferromagnetically; in most cases AFM ordering is more favorable. Ferromagnetic ordering of TM ions is not induced by the addition of substitutional Cu impurities nor by oxygen vacancies. Incorporation of interstitial or substitutional Li is favorable for ferromagnetism, as are Zn vacancies. On a technical note, we find that the calculated magnetic behavior is strongly dependent both on the computational details (with ferromagnetism disfavored by improved convergence) and on the choice of exchange-correlation functional (with ferromagnetism disfavored by the more appropriate LSDA+U method). This observation explains the large spread of computational results in the literature.

Acknowledgments This work was funded by the Department of Energy, grant number DE-FG03-02ER4598, and was partially supported by the MRSEC Program of the National Science Foundation under Award No. DMR05-20415. The authors thank Dr. Rebecca Janisch for useful discussions.

APPENDIX: DEPENDENCE OF PROPERTIES ON CHOICE OF U : THE EXAMPLE OF CO-DOPED ZNO

Here we illustrate the sensitivity of our results to the magnitude of the U parameter with calculations of the energy difference, $E_{AFM} - E_{FM}$ and total and orbital-resolved densities of states, as a function of U in the (Zn,Co)O system. The results are plotted in Figure 14. Figure 14: (upper panel) shows $E_{AFM} - E_{FM}$ for the LSDA case (with $U=0$, (i)), for U on the Co d states ranging from 4 to 6 eV (points (ii), (iii) and (iv)) and with a U of 4 eV on both the Co and Zn d states (v). Two conclusions can be drawn from the plot: First, the sign of the magnetic interaction changes from LSDA to LSDA+ U in the *near* case making the AFM ordering more stable. The AFM remains stable for a range of U values. Second, the U on the Co ion dominates the magnetic interaction; the energy differences in cases (ii) and (v) are very close, indicating that correlations on the Zn d states do not significantly affect the magnetic interactions. Figure 14 (lower panel) shows the DOS and Co d PDOS in Co-doped ZnO for a range of U values. We see that, as expected, the exchange splitting between occupied majority states, and unoccupied minority states increases with U ; as a consequence the majority occupied states move down into the valence band and hybridize more strongly with the O $2p$ states as U is increased. Adding a U of 4.5 eV on the Zn also lowers the energy of the Zn d states.

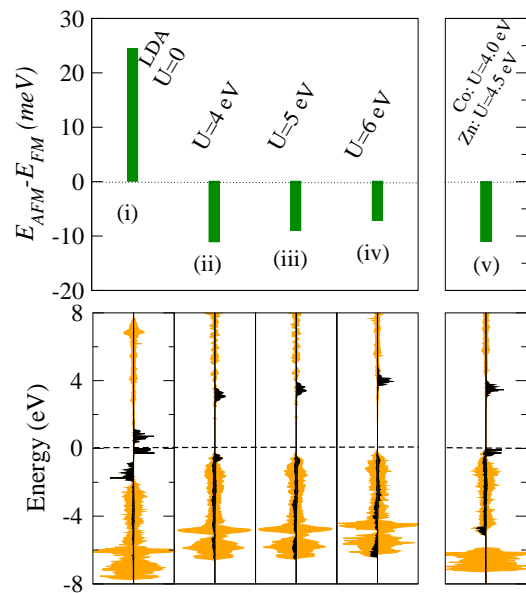


FIG. 14: Upper panel: Total energy difference (E_{AFM-FM}) for 12.5% Co in ZnO for various U values on the Co d states. The last bar gives this energy difference with $U = 4$ eV on both Zn and Co $3d$ states. The gray shaded and the black shaded bars show the energy differences for the *near* and *far* cases. Lower panel: Total DOS of (Zn,Co)O and PDOS of Co d states for a range of U values. The light shaded regions represent the total DOS while the black shaded regions correspond to the $3d$ states of Co ion.

- ¹ H. Ohno, *Science* **281**, 951 (1998).
- ² J. Furdyna, *J. Appl. Phys.* **64**, R29 (1988).
- ³ H. Saito, W. Zaets, S. Yamagata, Y. Suzuki, and K. Ando, *J. Appl. Phys.* **91**, 8085 (2002).
- ⁴ K. Ku, J. Potashnik, R. Wang, S. Chun, P. Schiffer, N. Samarth, M. Seong, A. Mascarenhas, E. Johnston-Halperin, and R. Myers, *Appl. Phys. Lett.* **82**, 2302 (2003).
- ⁵ T. Dietl, H. Ohno, F. Matsukara, J. Cibert, and D. Ferrand, *Science* **287**, 1019 (2000).
- ⁶ S. Sanvito, P. Ordejon, and N. A. Hill, *Phys. Rev. B* **63**, 165206 (2001).
- ⁷ *Landolt-Börnstein - Group III Condensed Matter* (Springer-Verlag, Heidelberg, 2002).
- ⁸ D. Norton, Y. Heo, M. Ivill, K. Ip, S. Pearton, M. Chisholm, and T. Steiner, *Materials Today* **6**, 34 (2004).
- ⁹ D. C. Look, *Mater. Sci. Eng. B* **80**, 383 (2001).
- ¹⁰ D. C. Look, R. Jones, J. Sizelove, N. Garces, N. Giles, and L. Haliburton, *Phys. Status Solidi (a)* **195**, 171 (2003).
- ¹¹ N. A. Hill and U. V. Waghmare, *Phys. Rev. B* **62**, 8802 (2000).
- ¹² V. E. Wood and A. E. Austin, *Magnetoelectric interaction phenomena in crystals* (Gordon and Breach, 1975).
- ¹³ P. Gopal and N. A. Spaldin, *J. Elect. Mater.: Special Issue* **35**, 538 (2006).
- ¹⁴ S. Ghosh, V. Sih, W. H. Lau, D. D. Awschalom, S. Y. Bae, S. Wang, S. Vaidya, and G. Chapline, *Appl. Phys. Lett.* **86**, 232507 (2005).
- ¹⁵ K. Ueda, H. Tabata, and T. Kawai, *Appl. Phys. Lett.* **79**, 988 (2001).
- ¹⁶ M. Venkatesan, C. B. Fitzgerald, J. C. Lunney, and J. M. D. Coey, *Phys. Rev. Lett.* **93**, 177206 (2004).
- ¹⁷ M. H. F. Sluiter, Y. Kawazoe, P. Sharma, A. R. Inoue, Raju, C. Rout, and U. V. Waghmare, *Phys. Rev. Lett.* **94**, 187204 (2005).
- ¹⁸ T. Fukumura, Z. Jin, A. Ohtomo, H. Koinuma, and M. Kawasaki, *Appl. Phys. Lett.* **75**, 3366 (1999).
- ¹⁹ S. Jung, S. J. An, G. C. Yi, C. Jung, S.-I. Lee, and S. Cho, *Appl. Phys. Lett.* **80**, 4561 (2002).
- ²⁰ P. Sharma, A. Gupta, K. V. Rao, F. J. Owens, R. Sharma, R. Ahuja, J. M. Osorio-Guillen, and G. A. Gehring, *Nat. Mater.* **2**, 673 (2003).
- ²¹ C. Song, K. W. Geng, F. Zeng, X. B. Wang, Y. Shen, F. Pan, Y. Xie, T. Liu, H. T. Zhou, and F. Fan, *Phys. Rev. B* **73**, 024405 (2006).
- ²² A. Risbud, N. Spaldin, Z. Chen, S. Stemmer, and R. Shadri, *Phys. Rev. B* **68**, 205202 (2003).
- ²³ K. R. Kittilsved, N. Norberg, and D. Gamelin, *Phys. Rev. Lett.* **94**, 147209 (2005).
- ²⁴ R. Janisch, P. Gopal, and N. A. Spaldin, *J. Phys. Condens.*

- Matter **17**, R657 (2005).
- ²⁵ S. Thota, T. Dutta, and J. Kumar, *J. Phys.: Condens. Matter* **18**, 2473 (2006).
- ²⁶ M. S. Park and B. I. Min, *Phys. Rev. B* **68**, 224436 (2003).
- ²⁷ K. Sato and H. Katayama-Yoshida, *Jpn. J. Appl. Phys* **39**, L555 (2000).
- ²⁸ P. Bruno and L. M. Sandratskii, *Phys. Rev. B* **73**, 045203 (2006).
- ²⁹ N. A. Spaldin, *Phys. Rev. B* **69**, 125201 (2004).
- ³⁰ C. H. Patterson, *cond-mat/0512101*.
- ³¹ L. Petit, T. C. Schulthess, A. Svane, Z. Szotek, W. M. Temmerman, and A. Janotti, *Phys. Rev. B* **73**, 045107 (2006).
- ³² E.-C. Lee and K. Chang, *Phys. Rev. B* **69**, 08205 (2004).
- ³³ Y. W. Heo, M. P. Ivill, K. Ip, D. P. Norton, and S. Pearton, *Appl. Phys. Lett.* **84**, 2292 (2003).
- ³⁴ Y. W. Yoon, S. B. Cho, S. C. We, B. J. Yoon, S. Suh, S. H. Song, and Y. J. Shin, *J. Appl. Phys.* **93**, 7879 (2003).
- ³⁵ J. Kim, W. K. Choo, H. Kim, D. Kim, and Y. Ihm, *J. Korean Phys. Soc.* **42**, S258 (2003).
- ³⁶ S. Kolesnik, B. Dabrowski, and J. Mais, *J. Appl. Phys.* **95**, 2582 (2004).
- ³⁷ J. M. D. Coey, M. Venkatesan, and C. Fitzgerald, *Nat. Mater.* **4**, 173 (2005).
- ³⁸ U. Özgür, Y. I. Alivov, C. Liu, A. Teke, M. A. Reshchikov, S. Doğan, V. Avrutin, S. J. Cho, and H. Morkoc, *J. Appl. Phys.* **98**, 041301 (2005).
- ³⁹ J. Shim, T. Hwang, J. Park, S. J. Han, and Y. Jeong, *Appl. Phys. Lett.* **86**, 082503 (2005).
- ⁴⁰ K. Ando, H. Saito, Z. Jin, F. Fukumura, M. Kawasaki, Y. Matsumoto, and H. Koinuma, *J. Appl. Phys.* **89**, 7284 (2001).
- ⁴¹ P. E. Blöchl, *Phys. Rev. B* **50**, 17953 (1994).
- ⁴² G. Kresse and J. Furthmüller, *Phys. Rev. B* **61**, 11169 (1996).
- ⁴³ G. Kresse and J. Furthmüller, *Comput. Mat. Sci.* **6**, 15 (1996).
- ⁴⁴ G. Kresse and J. Joubert, *Phys. Rev. B* **59**, 1758 (1999).
- ⁴⁵ R. Janisch and N. A. Spaldin, *Phys. Rev. B* **73**, 035201 (2006).
- ⁴⁶ V. Anisimov, F. Aryasetiawan, and A. Lichtenstein, *J. Phys.: Condens. Matter* **9**, 767 (1997).
- ⁴⁷ R. Powell and W. E. Spicer, *Phys. Rev. B* **2**, 2185 (1970).
- ⁴⁸ W. C. Messick, L. Walker and R. Glosser, *Phys. Rev. B* **6**, 3941 (1972).
- ⁴⁹ G. Sawatzky and J. Allen, *Phys. Rev. Lett.* **53**, 2239 (1984).
- ⁵⁰ S. Hüfner, I. Sander, F. Reinert, and H. Schnitt, *J. Phys. B.:Condens. Matter* **86**, 207 (1992).
- ⁵¹ J. v. Elp, H. Eskes, P. Kuiper, and G. A. Sawatzky, *Phys. Rev. B* **207**, 1612 (1992).
- ⁵² K. Terakura, T. Oguchi, A. R. Williams, and J. Kübler, *Phys. Rev. B* **30**, 4734 (1984).
- ⁵³ V. Anisimov, J. Zaanen, and O. Anderson, *Phys. Rev. B* **44**, 943 (1991).
- ⁵⁴ W. E. Pickett, S. C. Erwin, and E. C. Ethridge, *Phys. Rev. B* **58**, 1201 (1998).
- ⁵⁵ M. Cococcioni and S. Gironcoli de, *Phys. Rev. B* **71**, 035105 (2005).
- ⁵⁶ M. Park and B. Min, *Phys. Rev. B* **68**, 224436 (2003).
- ⁵⁷ P. W. Anderson, *Phys. Rev.* **79**, 350 (1950).
- ⁵⁸ J. B. Goodenough, *Phys. Rev.* **100**, 564 (1955).
- ⁵⁹ J. Kanamori, *J. Phys. Chem. Solids* **10**, 87 (1958).
- ⁶⁰ R. D. Shannon and C. T. Prewitt, *Acta Crystallogr. Sect. A: Cryst. Phys. Diffr., Theor. Gen. Crystallogr.* **32**, 751 (1976).
- ⁶¹ S. J. Han, J. W. Song, C. H. Yang, C. H. Park, J. H. Park, Y. H. Jeong, and K. W. Rhite, *Appl. Phys. Lett.* **81**, 4212 (2002).
- ⁶² A. F. Kohan, G. Ceder, D. Morgan, and C. G. V. de Walle, *Phys. Rev. B* **61**, 15019 (2000).
- ⁶³ A. Onodera, K. Yoshio, H. Satoh, H. Yamashita, and N. Sakagami, *Jpn. J. Appl. Phys.* **1998**, 5315 (1998).
- ⁶⁴ T. Nagata, T. Shimura, Y. Nakano, A. Ashida, N. Fujimura, and T. Ito, *Jpn. J. Appl. Phys.* **40**, 5615 (2001).
- ⁶⁵ S. Zhang, W. S., and A. Zunger, *Phys. Rev. B* **63**, 075205 (2001).
- ⁶⁶ F. Tuomisto, K. Saarinen, D. C. Look, and G. Farlow, *Phys. Rev. B* **72**, 085206 (2005).
- ⁶⁷ M. Naeem, S. K. Hasanain, M. Kobayashi, Y. Ishida, A. Fujimori, S. Buzby, and S. Ismat, *cond-mat/0512597*.
- ⁶⁸ A. Janotti and C. G. Van de Walle, *Appl. Phys. Lett.* **87**, 122102 (2005).
- ⁶⁹ S. G. Yang, A. B. Pakhmov, S. T. Hung, and C. Y. Wong, *IEEE Trans. Magn.* **38**, 2877 (2002).
- ⁷⁰ Y. M. Cho, W. K. Choo, H. Kim, D. Kim, and Y. Ihm, *Appl. Phys. Lett.* **80**, 3358 (2002).
- ⁷¹ E. Lee and K. J. Chang, *Phys. Rev. B* **69**, 0285205 (2004).